Proceedings of the
Annual Stability Conference
Structural Stability Research Council
Louisville, Kentucky, April 1-4, 2025

Local stability of 3D-printed stainless steel channel sections under compression

Xi Chen[1], Kaiyang Wang[2], Yao Sun[3]

Abstract
Additive manufacturing, often known as 3D printing, is being used in the construction sector. This paper reports an experimental study on the compression resistances and local stability of 3D-printed stainless steel channel sections. The experimental study includes material coupon tests, measurements of geometric properties and stub column tests on stainless steel channel sections that were 3D-printed by means of wire-arc additive manufacturing. The obtained test results were used in an in-depth design analysis, where the applicability of the European and American standards as well as the continuous strength method to 3D-printed stainless steel channel sections was assessed. The design analysis results indicate that the current international standards offer satisfactory design accuracy for 3D-printed stainless steel stub columns with slender channel sections, but yield rather conservative resistance predictions for their slender counterparts. It is found that the continuous strength method offers greatly improved design accuracy over the considered international standards, due to the consideration of material strain hardening.

1. Introduction
The construction industry is undergoing a transformative shift toward innovation and automation, with additive manufacturing (AM), also known as 3D printing, playing a pivotal role in this process (Wu et al. 2016, Buchanan and Gardner 2019, Gardner 2023, Sun 2023). Among the various AM techniques, wire-arc additive manufacturing (WAAM) is gaining attention for its potential to produce large-scale metal components for structural applications (Buchanan and Gardner 2019, Evans et al. 2022). WAAM employs wire feedstocks and electric arc welding tools to create components layer by layer, offering advantages such as high deposition rates, cost efficiency, design flexibility, structural integrity, and lower environmental impact compared to traditional methods (El-Sayegh et al. 2020, Lange et al. 2020, Shah et al. 2023). These attributes make WAAM especially suitable for stainless steel. Despite these benefits, WAAM stainless steel components face challenges, including variability in mechanical properties, structural inconsistencies, and surface imperfections, such as roughness and geometric distortions, which require further research for their application in the structural engineering sector.

[1] Postdoctoral Research Fellow, College of Civil Engineering, Hunan University, <xichen23@hnu.edu.cn>
[2] Associate Professor, College of Civil Engineering, Nanjing Forestry University, <kaiyang.wang@njfu.edu.cn>
[3] Full Professor, College of Civil Engineering, Hunan University, (corresponding author) <yaosun@hnu.edu.cn>

Experimental investigations into WAAM stainless steel have primarily focused on material properties and structural performance. Studies have explored the effects of factors like material grades, plate thicknesses, surface conditions, and specimen orientations on tensile and compressive responses, revealing material anisotropy linked to crystallographic texture (Kyvelou et al. 2020, Laghi et al. 2020b, Hadjipantelis et al. 2022, Zhao et al. 2023). At the structural level, researchers have examined the local stability and compressive capacities of circular and square hollow sections, I-sections as well as the flexural response of tubular beams (Laghi et al. 2020a, Kyvelou et al. 2021, Zhang et al. 2021, Feng et al. 2022, Huang et al. 2022, Huang et al. 2023). These studies highlighted variability in performance between specimens and identified discrepancies between experimental results and predictions by international design standards. However, existing research has largely centred on doubly symmetric cross-sections, leaving a significant gap in understanding the behaviour of singly symmetric (e.g., channel and equal-leg angle) and asymmetric (e.g. unequal-leg angle) profiles. The only relevant research was performed by Evans et al. (2023) and Evans et al. (2024), where WAAM equal-leg angle section stub columns were studied.

To address this research gap, this paper presents an experimental investigation of the cross-sectional capacity of WAAM stainless steel stub columns with channel sections. The study includes detailed specimen preparation, geometry measurements, material testing, and a series of fifteen stub column tests using EN 1.4404 stainless steel channel sections. Furthermore, the experimental results are compared against existing design standards, including prEN 1993-1-4 (2023), AISC 370-21 (2021), and the Continuous Strength Method (CSM) (Gardner et al. 2023), to evaluate their applicability to WAAM stainless steel structures. The findings provide valuable insights into advancing the design and application of WAAM stainless steel in structural engineering.

2. Fabrication of Test Specimens

The WAAM stainless steel channel sections used in this study were fabricated using advanced robotic 3D printing technology. The sections were produced with a KUKA R1810 robotic printer, employing 1.2 mm diameter EN 1.4404 austenitic stainless-steel wire as the feed material, with power supplied by a Fronius TPS 400i system. The layers were printed perpendicular to the longitudinal axis of the channel sections. Three nominal material thicknesses—3.5 mm, 4.5 mm, and 6.0 mm—were selected, and the key manufacturing parameters are presented in Table 1.

Table 1: Key parameters for WAAM process

Voltage	Current	Layer height	Wire feed speed	Travel speed	Nozzle temperature	Gas flow rate
11.4 V	111 A	1.4 mm	3.7 m/min	0.0133 m/min	200 ℃	20 L/min

2.1 Fabrication of Coupons

Coupons were extracted from both the flanges and webs of the WAAM channel sections for material testing. Two coupons were prepared for each of the three thicknesses, ensuring they were cut longitudinally (perpendicular to the deposition direction, as shown in Fig. 1) using wire-cut electrical discharge machining (EDM). To minimise surface irregularities, the central portion of each coupon was machined to achieve uniform thickness, and burrs were removed to comply with GB/T 228-1 (SAC 2021) standards.

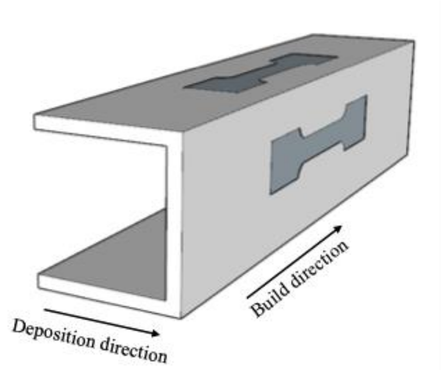

Figure 1: Extraction of WAAM coupons (Note: Deposition direction is in the plane of the layer; build direction is the direction that the layers are stacking.)

2.2 Fabrication of Stub Columns

Fifteen stub columns were fabricated from WAAM channel sections with five different channel profiles (C-50×35, C-65×40, C-80×45, C-100×50 and C-120×65), each produced in three thicknesses (3.5 mm, 4.5 mm, and 6.0 mm). The column lengths were determined following Ziemian (2010), calculated as three times the mean of the section height and flange width to include representative imperfection patterns while avoiding global buckling. Surface imperfections, such as large droplets from the printing process, were removed by machining to ensure consistency in specimen geometry.

3. Testing Program and Experimental Results

Following the fabrication of WAAM stainless steel coupons and stub columns, a comprehensive testing program was undertaken to evaluate their cross-sectional behaviour and capacity under compression. This program included six material coupon tests, geometric property measurements and fifteen stub column compression tests.

3.1 Material Testing

Tensile coupon tests were conducted using an INSTRON 100 kN displacement-controlled machine, following GB/T 228-1 guidelines (SAC 2021). Three pairs of coupons representing different thicknesses were tested. The initial loading rate was 0.05 mm/min, increasing to 0.40 mm/min upon reaching 0.2% proof strength (Sun et al. 2024,2025). Strains were monitored using a digital image correlation (DIC) system, which captured localised strain concentrations leading to fractures in the gauge length. The measured stress-strain curves are displayed in Fig. 2, which demonstrate negligible variation across thicknesses and are consistent with findings in prior research on 3D-printed stainless steels (Kyvelou et al. 2020, Evans et al. 2023). The average key material properties, including Young’s modulus, proof strength, ultimate strength, and fracture strain, are summarised in Table 2.

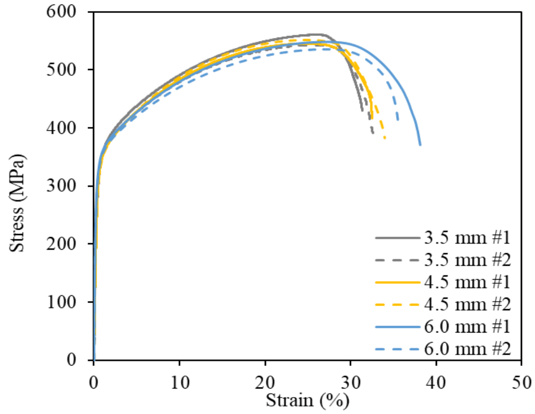

Figure 2: Measured stress–strain curves

Table 2: Key measured material properties of WAAM stainless steel

Plate thickness (mm)	E (GPa)	f_y (MPa)	f_u (MPa)	f_u/f_y	ε_u (%)	ε_f (%)	n	m
3.5	191.0	300.1	551.4	1.84	25.9	32.9	4.5	2.5
4.5	190.7	304.2	548.2	1.80	24.7	33.8	3.4	2.6
6.0	188.9	303.8	541.8	1.78	27.2	37.3	3.8	2.6

3.2 Measurements of Geometric Properties

Geometric properties of the stub columns were measured using a HEXAGON CMS 108 3D laser scanner, with point cloud data processed into '.stl' models and visualised in Rhinoceros 3D. Cross-sectional dimensions and local imperfections were evaluated at five evenly spaced sections along each column length, as the scanned stub column specimen C-120×65×6 is shown as an example in Fig. 3. Measurements such as section height, flange width, plate thickness, and initial imperfections were derived from the data points to reveal geometric deviations caused by the additive manufacturing process. Geometric dimensions for the WAAM stub columns are listed in Table 3, with an overall fabrication accuracy of ±2.1% compared to nominal dimensions.

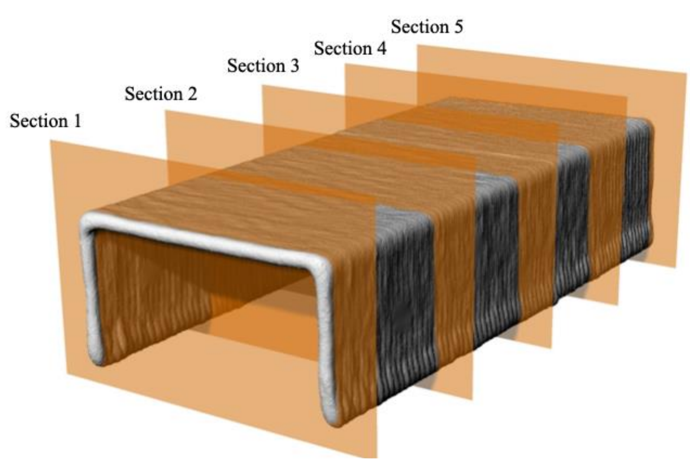

Figure 3: Cross-section extraction of scanned specimen C-120×65×6

Table 3. Geometric dimensions of WAAM stainless steel stub column specimens

Specimen ID	L (mm)	h (mm)	b_f (mm)	t_w (mm)	t_f (mm)	ω_o (mm)
C-50×35×3.5	118.4	49.7	35.6	3.44	3.42	0.35
C-50×35×4.5	119.6	49.5	36.1	4.52	4.52	0.33
C-50×35×6	118.2	49.2	35.2	5.66	5.72	0.43

C-65×40×3.5	144.2	64.8	40.8	3.52	3.56	0.22
C-65×40×4.5	144.4	64.2	41.2	4.54	4.52	0.32
C-65×40×6	144.1	64.4	41.2	5.62	5.74	0.37
C-80×45×3.5	171.8	78.2	44.6	3.42	3.46	0.34
C-80×45×4.5	170.1	79.2	45.8	4.52	4.52	0.44
C-80×45×6	169.6	79.1	45.6	5.64	5.72	0.30
C-100×50×3.5	201.5	97.4	49.6	3.36	3.32	0.37
C-100×50×4.5	200.1	98.1	50.4	4.41	4.43	0.49
C-100×50×6	200.7	99.2	51.6	5.60	5.72	0.44
C-120×65×3.5	251.2	119.2	64.4	3.44	3.38	0.33
C-120×65×4.5	251.4	118.9	65.4	4.48	4.48	0.45
C-120×65×6	250.2	119.2	65.1	5.62	5.72	0.39

3.3 Stub Column Tests

Stub column compression tests were performed on fifteen specimens across five channel profiles, with three thicknesses each. The stub columns, pre-milled for flat ends and deburred for uniform stress distribution, were subjected to concentric compressive loads using a machine with fixed-ended boundary conditions. The test setup is displayed in Fig. 4, including three LVDTs and three strain gauges to measure end-shortening and longitudinal strains. A loading rate of 0.30 mm/min (Sun et al. 2019, Ran et al. 2024) was applied to each stub column ensuring consistent application of forces. The load–end-shortening behaviour of the stub columns across five channel section profiles is illustrated in Fig. 5, with key results presented in Table 4. These include ultimate loads (N_u), end-shortenings (δ_u), and ultimate-to-yield load ratios ($N_u/(Af_y)$), where A represents the gross cross-section area. As shown in Fig. 6, the stub column specimens exhibited notable localised deformations, characterized by a classic "in-out" deformation mode at the mid-height cross-section.

Figure 4: Stub column test setup

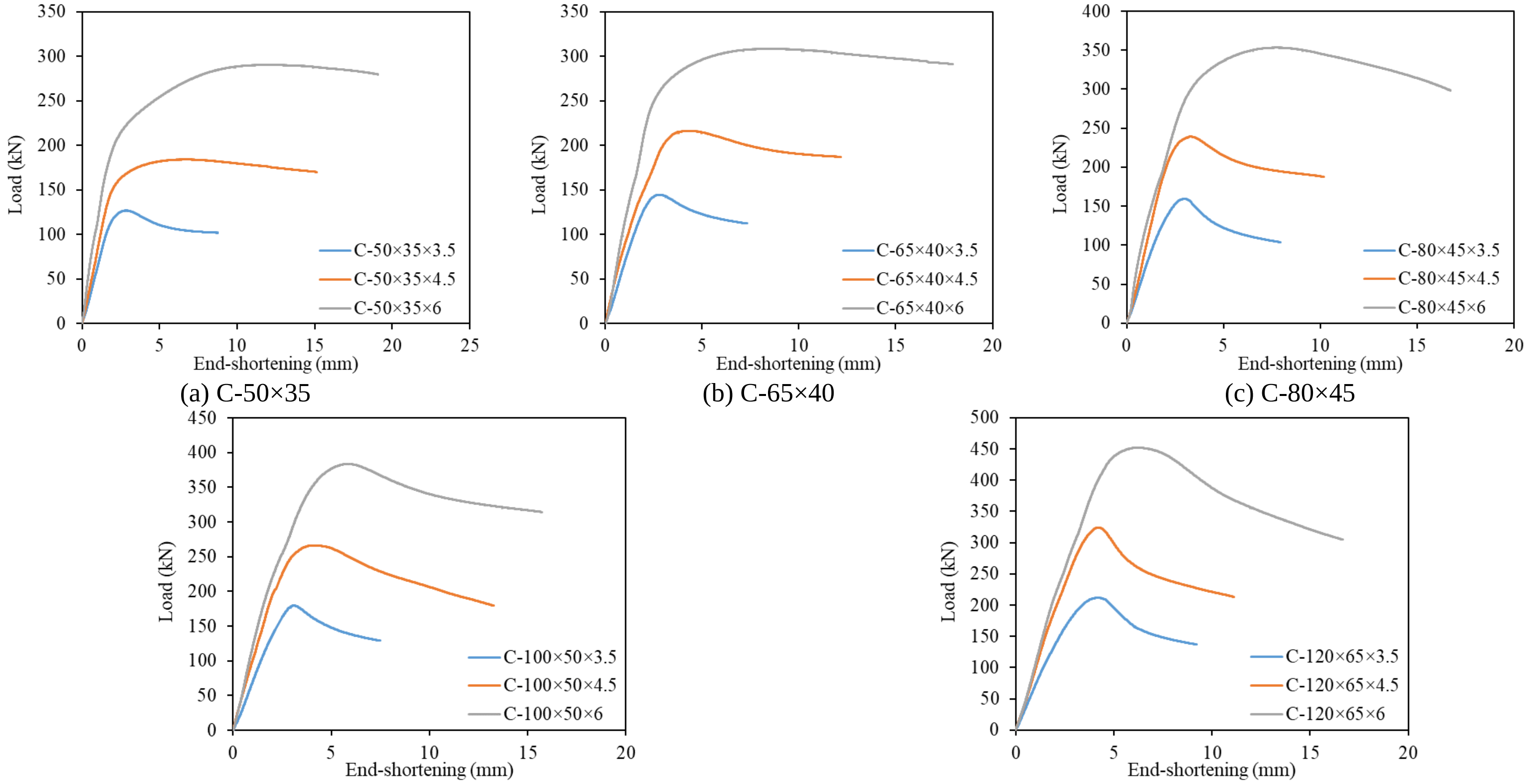

(a) C-50×35 (b) C-65×40 (c) C-80×45

(d) C-100×50 (e) C-120×65

Figure 5: Load–end-shortening curves for tested WAAM stub columns

Table 4. Key stub column test results

Specimen ID	N_u (kN)	δ_u (mm)	$N_u / (Af_y)$
C-50×35×3.5	126.9	2.82	1.08
C-50×35×4.5	184.3	6.64	1.19
C-50×35×6	290.3	11.75	1.66
C-65×40×3.5	144.7	2.83	0.98
C-65×40×4.5	216.4	4.27	1.14
C-65×40×6	308.3	8.49	1.41
C-80×45×3.5	159.6	3.01	0.96
C-80×45×4.5	239.2	3.33	1.08
C-80×45×6	353.6	7.66	1.38
C-100×50×3.5	179.4	3.11	0.94
C-100×50×4.5	266.4	4.10	1.04
C-100×50×6	383.7	5.85	1.25
C-120×65×3.5	211.6	4.19	0.86
C-120×65×4.5	324.4	4.32	0.99
C-120×65×6	452.5	6.34	1.18

Figure 6: Failure modes of tested WAAM stub columns

4. Design Analysis

Using experimental test data, a design analysis is performed to evaluate the applicability of existing design standards for conventionally manufactured stainless steel structures to WAAM stainless steel channel section stub columns, including prEN 1993-1-4 (2023), AISC 370-21 (2021), and the Continuous Strength Method (CSM) (Gardner et al. 2023). Table 5 summarises the mean test-to-predicted ultimate load ratios ($N_u/N_{u,pred}$) and coefficients of variation (CoVs) for each design method. These predicted values are given in the Table as $N_{u,EC3}$, $N_{u,AISC}$ and $N_{u,CSM}$, for prEN 1993-1-4, AISC 370-21 and the CSM (Gardner et al. 2023), respectively. Figs. 7–11 show graphical comparisons of the load ratios against the width-to-thickness ratio of the channel flange, i.e. $(b_f-t_w)/t_f$.

Table 5. Evaluation of existing design method

Cross-section	$N_u/N_{u,EC3}$		$N_u/N_{u,AISC}$		$N_u/N_{u,CSM}$	
	Mean	CoV	Mean	CoV	Mean	CoV
Non-slender	1.263	0.150	1.257	0.155	1.072	0.044
Slender	1.066	0.050	1.062	0.046	0.996	0.015
Overall	1.184	0.150	1.179	0.153	1.040	0.053

4.1 prEN 1993-1-4

For prEN 1993-1-4 (2023), the Eurocode classifies sections into slender (Class 4) or non-slender (Classes 1–3) based on plate width-to-thickness ratios relative to material parameters. Non-slender sections are assumed to reach their yield loads (Af_y), whereas slender sections experience local instability before achieving Af_y. This classification relies on the Class 3 slenderness limits derived from their width-to-thickness ratios, which is 11.5ε for flanges and 35.4ε for webs, where $\varepsilon = (235/f_y)^{0.5}$ is the material parameter. The test results for WAAM stainless steel channel sections indicate that the current slenderness limit for internal webs (Fig. 7(a)) fails to accurately distinguish between Class 4 sections (i.e. those with $N_u/(Af_y) < 1$) and Class 1–3 non-slender sections (i.e. those with $N_u/(Af_y) \geq 1$), while the slenderness limits effectively classify the channel flanges (Fig. 7(b)).

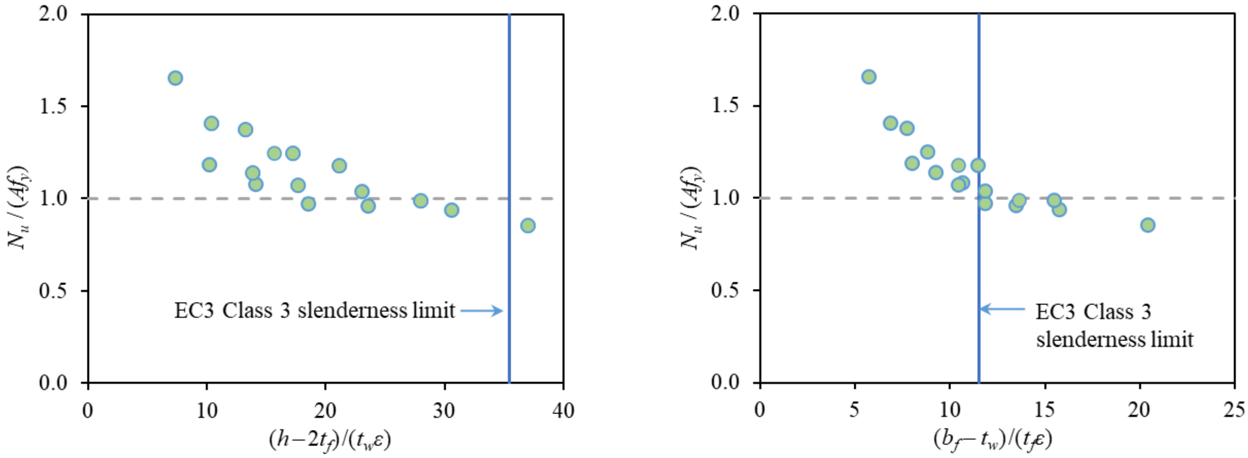

(a) Internal webs (b) Outstand flanges

Figure 7: Assessment of EC3 Class 3 slenderness limits

Design compression resistances are determined using yield load Af_y for non-slender sections and effective load $A_{eff}f_y$ for slender sections, with A_{eff} calculated using the effective width method accounting for local instability. The effective width c_{eff} is calculated as the original plate width c (taken as $h-2t_f$ and b_f-t_w for webs and flanges, respectively) multiplied by the reduction factor ρ_{EC3} that is given in Eq. (1), where λ_p is the plate slenderness, as calculated from Eq. (2), in which k_σ is the buckling factor and respectively equal to 0.43 and 1.0 for flanges and webs.

$$\rho_{EC3} = \begin{cases} \dfrac{0.655\lambda_p - 0.012}{\lambda_p^{\ 2}} & \text{for webs} \\ \dfrac{0.655\lambda_p - 0.01}{\lambda_p^{\ 2}} & \text{for flanges} \end{cases} \tag{1}$$

$$\lambda_p = \frac{c/t}{27.7\varepsilon\sqrt{k_\sigma}} \tag{2}$$

However, when applied to WAAM stainless steel, the prEN 1993-1-4 provisions show varying levels of accuracy, as shown in Table 5. For Class 4 slender sections, the design predictions are reasonably accurate, with a mean ultimate load ratio of $N_u/N_{u,EC3}$ = 1.066, indicating minimal deviation from the experimental results. Conversely, for non-slender Classes 1–3 sections, the code significantly underestimates the load-carrying capacity, with a mean mean $N_u/N_{u,EC3}$ ratio of 1.263, highlighting its conservative nature. The conservatism in the predictions for non-slender sections is mainly induced by the code's inability to account for the strain-hardening behaviour of WAAM stainless steel, which improves the load-carrying capacity of stockier sections. This limitation is evident in Fig. 8, where the load ratios $N_u/N_{u,EC3}$ are plotted against the slenderness parameter $(b_f - t_w)/t_f$. The results indicate the need for modifications in the Eurocode to better reflect the unique mechanical behaviour of WAAM stainless steel, particularly for non-slender sections where strain-hardening plays a significant role.

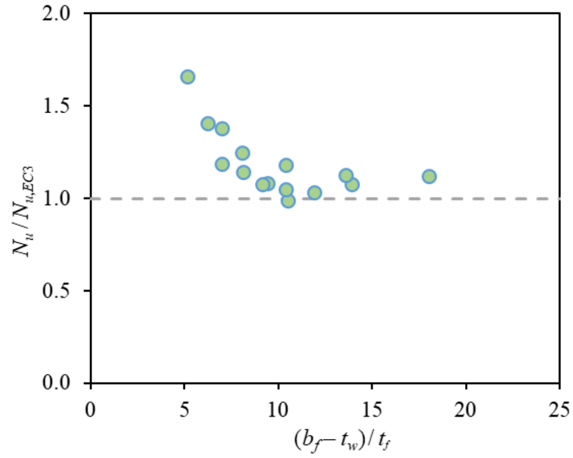

Figure 8: Comparison of test and EC3 predicted failure loads

4.2 AISC 370-21

AISC 370-21 (2021) is a American design standard for stainless steel structures. Similar to the Eurocode prEN 1993-1-4 (2023), AISC 370-21 classifies cross-sections under compression into slender and non-slender categories based on flange and web width-to-thickness ratios. For channel flanges, the width-to-thickness ratio ($\lambda = b_f/t_f$) is compared to a limiting value $\lambda_r = 0.41(E/f_y)^{0.5}$, while for webs, the ratio $\lambda = (h - 2t_f)/t_w$ is compared to $\lambda_r = 1.24(E/f_y)^{0.5}$. Non-slender sections are assumed to reach their full yield capacity Af_y, while slender sections are prone to local buckling, which reduces their effective cross-sectional area. To account for this, AISC employs the effective width method, where a reduction factor ρ_{AISC} adjusts the plate's original width to its effective width, as determined by Eq. 3. f_{el} in the equation is the elastic local buckling stress as per codified Eq. 4, in which $\nu = 0.3$ is the Poisson's ratio of stainless steel.

$$\rho_{AISC} = 0.772\left(1 - 0.10\sqrt{\frac{f_{el}}{f_y}}\right)\sqrt{\frac{f_{el}}{f_y}} \tag{3}$$

$$f_{el} = \frac{k_\sigma \pi^2 E}{12\left(1 - \nu^2\right)\lambda^2} \tag{4}$$

The suitability of AISC 370-21 for WAAM stainless steel channel sections was assessed both qualitatively and quantitatively using experimental results. Fig. 9 compares test failure loads normalised by yield loads with the AISC limiting ratios, revealing similar trends to the Eurocode's slenderness classifications: the flange limits show high accuracy, while those for webs fail to effectively separate slender and non-slender sections. The quantitative evaluation of compressive capacity, as summarised in Table 5, provides the mean ultimate load ratios ($N_u/N_{u,AISC}$) and CoVs for slender and non-slender channel sections. These results, along with the graphical assessments in Fig. 10, highlight that the AISC provision can accurately predict the compressive capacities of slender WAAM stainless steel sections, which are dominated by local buckling effects. However, it is conservative for non-slender WAAM sections, as the American provision does not account for the strain-hardening behaviour, which enhances the load-carrying capacity of stockier sections. Overall, AISC 370-21 demonstrates comparable accuracy to prEN 1993-1-4, with a mean load ratio $N_u/N_{u,AISC}$ = 1.179 versus $N_u/N_{u,EC3}$ = 1.184 for the European code.

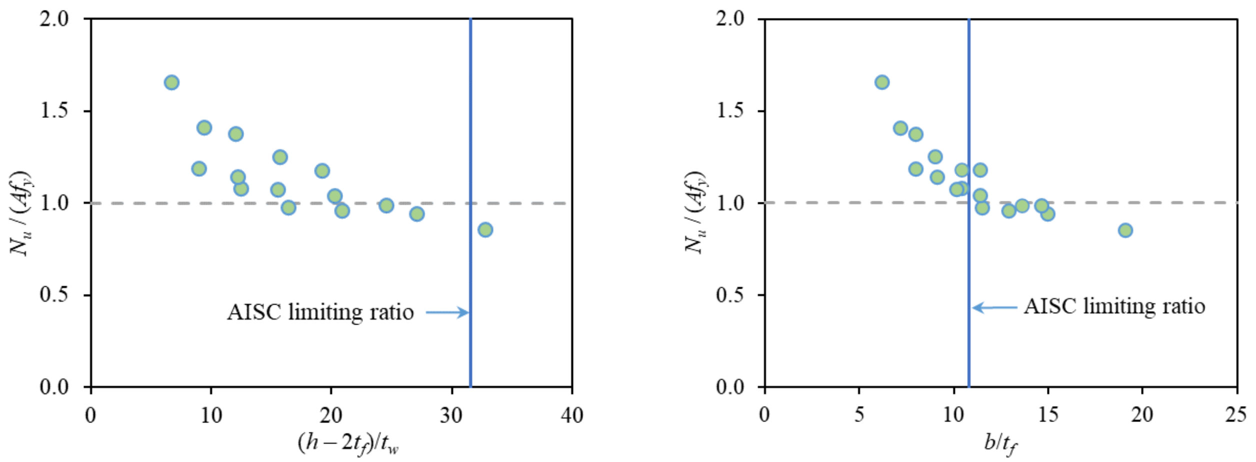

(a) Internal webs. (b) Outstand flanges.

Figure 9: Assessment of AISC limiting ratios

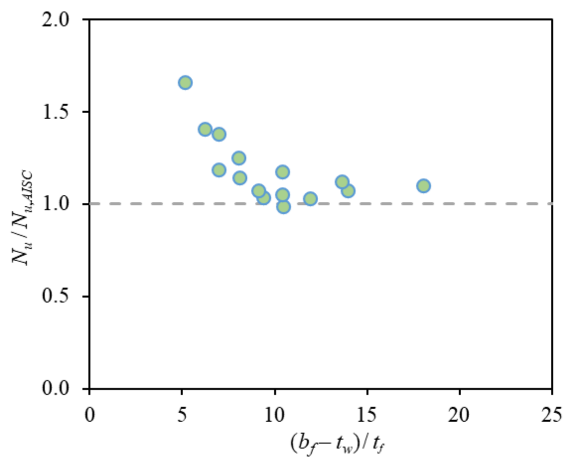

Figure 10: Comparison of test and AISC predicted failure loads

4.3 CSM

The findings in the previous sections highlight that existing international design standards tend to conservatively predict the capacities of WAAM stainless steel non-slender channel sections. This is attributed to their lack of consideration for the material strain-hardening behaviour. To address this limitation, the Continuous Strength Method (CSM) (Gardner et al. 2023), which incorporates strain hardening, has been adopted as an alternative design approach in both prEN 1993-1-4 (2023) and AISC 370-21 (2021). Initially proposed by Gardner (2008) and subsequently refined in later studies (Gardner 2019), the CSM has been successfully applied to stainless steel component design (Bock et al. 2015, Sun and Zhao 2019, Arrayago et al. 2020, Ran et al. 2023).

The CSM calculates the cross-sectional compressive capacity in two main steps. First, the CSM strain limit (ε_{csm}), representing the deformation capacity of the section, is determined using the 'base curve' (Eq. 7). $\varepsilon_y = f_y/E$ and $\lambda_{p,cs} = (f_{0.2}/f_{cr,cs})^{0.5}$ are the yield strain and the cross-sectional slenderness, respectively, where $f_{cr,cs}$ is the elastic local buckling stress of the channel section and can be derived using the finite-strip program CUFSM (Schafer and Adany 2006). Once ε_{csm} is established, the CSM compressive capacity $N_{u,CSM}$ is obtained from Eq. 8, in which E_{sh} is the strain-hardening modulus and is calculated using Eq. 9, and $\varepsilon_{u,csm} = 1–f_u/f_y$ is the ultimate strain.

$$\frac{\varepsilon_{csm}}{\varepsilon_y} = \begin{cases} \dfrac{0.25}{\lambda_{p,cs}^{3.6}} \le \min\left(15, \dfrac{0.1\varepsilon_u}{\varepsilon_y}\right) & \text{for } \lambda_{p,cs} \le 0.68 \\ \left(1 - \dfrac{0.222}{\lambda_{p,cs}^{1.05}}\right)\dfrac{1}{\lambda_{p,cs}^{1.05}} & \text{for } \lambda_{p,cs} > 0.68 \end{cases} \tag{7}$$

$$N_{u,CSM} = \begin{cases} Af_y \dfrac{\varepsilon_{csm}}{\varepsilon_y} & \text{for } \dfrac{\varepsilon_{csm}}{\varepsilon_y} \le 1.0 \\ Af_y + AE_{sh}\varepsilon_y\left(\dfrac{\varepsilon_{csm}}{\varepsilon_y} - 1\right) & \text{for } \dfrac{\varepsilon_{csm}}{\varepsilon_y} > 1.0 \end{cases} \tag{8}$$

$$E_{sh} = \frac{f_u - f_y}{0.16\varepsilon_{u,csm} - \varepsilon_y} \tag{9}$$

The experimental results validate the efficiency of the CSM in predicting ultimate loads. In Fig. 11, the experimental ultimate loads N_u normalised by the corresponding $N_{u,CSM}$, values are plotted against the cross-sectional slenderness $\lambda_{p,cs}$, demonstrating excellent agreement between test and predicted capacities. This qualitative evaluation is complemented by the quantitative analysis results as summarised in Table 5, with the mean $N_u/N_{u,csm}$ ratios of 0.996 for slender sections and 1.072 for non-slender sections.

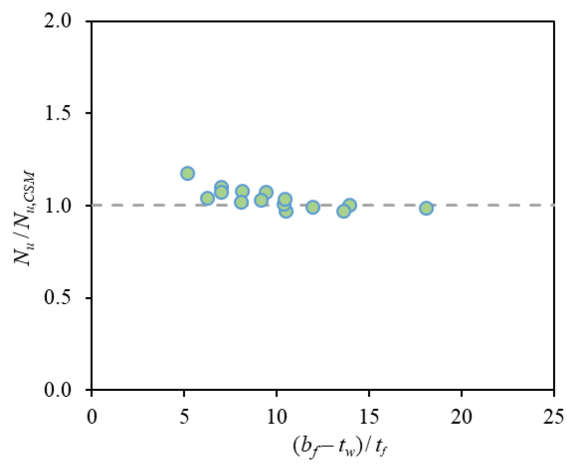

Figure 11: Comparison of test and CSM predicted failure loads

5. Conclusions

The compressive load-carrying capacity of WAAM stainless steel channel sections has been systematically investigated through an experimental program comprising material tests, geometry measurements, and fifteen stub column tests. These tests revealed consistent local instability across all specimens, characterized by significant localized deformation. The experimental findings were subsequently utilized to assess the applicability of various design standards, including the European prEN 1993-1-4, American AISC 370-21 and the Continuous Strength Method (CSM), to WAAM stainless steel channel sections. The key conclusions drawn from the study are as follows:

(i) The slenderness limits defined in prEN 1993-1-4 and AISC 370-21 were found to accurately distinguish between slender and non-slender flanges. However, the same codified limits were less effective for the classification of webs, highlighting an area where the design standards could be improved for WAAM stainless steel components.
(ii) For slender channel sections, the codified provisions generally yielded reasonably accurate predictions of compressive capacities. The mean ratios of test-to-predicted ultimate loads were $/N_{u,EC3} = 1.066$ and $N_u/N_{u,AISC} = 1.062$, indicating the adequacy of the existing design standards for slender sections. However, for non-slender channel sections, significant conservatism was observed in the predictions from both examined codes, with mean ratios of $N_u/N_{u,EC3} = 1.263$ and $N_u/N_{u,AISC} = 1.257$. This conservatism is attributed to the increasing influence of material strain hardening, which is not sufficiently considered in the design provisions.
(iii) The CSM design approach, which explicitly incorporates material strain-hardening effects, demonstrated the best overall consistency and accuracy in predicting compressive capacities. With an overall mean test-to-predicted load ratio of $N_u/N_{u,CSM} = 1.040$, the CSM offers a more reliable and rational design method for WAAM stainless steel channel sections, particularly for non-slender sections where strain hardening significantly influences the structural behaviour.

These findings demonstrate the need for enhanced design approaches that account for the unique material characteristics and behaviour of WAAM stainless steel, particularly its strain-hardening potential.

References

AISC (2021). ANSI/AISC 370-21: Specification for Structural Stainless Steel Buildings, American Institute of Steel Construction (AISC).

Arrayago, I., E. Real, E. Mirambell and L. Gardner (2020). "The Continuous Strength Method for the design of stainless steel hollow section columns." *Thin-Walled Structures*, 154.

Bock, M., L. Gardner and E. Real (2015). "Material and local buckling response of ferritic stainless steel sections." *Thin-Walled Structures*, 89 131-141.

Buchanan, C. and L. Gardner (2019). "Metal 3D printing in construction: A review of methods, research, applications, opportunities and challenges." *Engineering Structures*, 180 332-348.

CEN (2023). prEN 1993-1-4:2023: Eurocode 3 - Design of steel structures - Part 1-4: General rules - Supplementary rules for stainless steels. Brussels, Belgium, European Committee for Standardization (CEN).

El-Sayegh, S., L. Romdhane and S. Manjikian (2020). "A critical review of 3D printing in construction: benefits, challenges, and risks." *Archives of Civil and Mechanical Engineering*, 20(2) 34.

Evans, S., F. Xu and J. Wang (2023). "Material properties and local stability of WAAM stainless steel equal angle sections." *Engineering Structures*, 287 116160.

Evans, S. I., N. Hadjipantelis and J. Wang (2024). "Stub column tests on wire arc additively manufactured equal-leg angle sections." *Engineering Structures*, 317.

Evans, S. I., J. Wang, J. Qin, Y. He, P. Shepherd and J. Ding (2022). "A review of WAAM for steel construction – Manufacturing, material and geometric properties, design, and future directions." *Structures*, 44 1506-1522.

Feng, R., J.-P. Tang, W.-M. Quach, M. Yan and J. Zhao (2022). "Experimental study on additive manufactured 304L stainless steel tubular sections: Material properties and cross-sectional behavior." *Engineering Structures*, 273.

Gardner, L. (2008). "The continuous strength method." *Proceedings of the Institution of Civil Engineers - Structures and Buildings*, 161(3) 127-133.

Gardner, L. (2019). "Stability and design of stainless steel structures – Review and outlook." *Thin-Walled Structures*, 141 208-216.

Gardner, L. (2023). "Metal additive manufacturing in structural engineering – review, advances, opportunities and outlook." *Structures*, 47 2178-2193.

Gardner, L., X. Yun and F. Walport (2023). “The Continuous Strength Method – Review and outlook.” *Engineering Structures*, 275.
Hadjipantelis, N., B. Weber, C. Buchanan and L. Gardner (2022). “Description of anisotropic material response of wire and arc additively manufactured thin-walled stainless steel elements.” *Thin-Walled Structures*, 171.
Huang, C., X. Meng and L. Gardner (2022). “Cross-sectional behaviour of wire arc additively manufactured tubular beams.” *Engineering Structures*, 272.
Huang, Y., L. Yang, M. Liu and K. Xu (2023). “Local buckling of WAAM stainless steel circular columns.” *ce/papers*, 6(3-4) 775-780.
Kyvelou, P., C. Huang, L. Gardner and C. Buchanan (2021). “Structural Testing and Design of Wire Arc Additively Manufactured Square Hollow Sections.” *Journal of Structural Engineering*, 147(12) 04021218.
Kyvelou, P., H. Slack, D. Daskalaki Mountanou, M. A. Wadee, T. B. Britton, C. Buchanan and L. Gardner (2020). “Mechanical and microstructural testing of wire and arc additively manufactured sheet material.” *Materials & Design*, 192.
Laghi, V., M. Palermo, G. Gasparini, V. A. Girelli and T. Trombetti (2020a). “Experimental results for structural design of Wire-and-Arc Additive Manufactured stainless steel members.” *Journal of Constructional Steel Research*, 167 105858.
Laghi, V., M. Palermo, L. Tonelli, G. Gasparini, L. Ceschini and T. Trombetti (2020b). “Tensile properties and microstructural features of 304L austenitic stainless steel produced by wire-and-arc additive manufacturing.” *The International Journal of Advanced Manufacturing Technology*, 106 3693-3705.
Lange, J., T. Feucht and M. Erven (2020). “3D printing with steel.” *Steel Construction*, 13(3) 144-153.
Ran, H., Z. Chen, Y. Ma, L. Di Sarno and Y. Sun (2023). “Local stability of laser-welded stainless steel slender I-sections under combined loading.” *Journal of Constructional Steel Research*, 200, 107649.
Ran, H., J. Ma, X. Chen, Y. Sun, M. Gkantou and D. McCrum (2024). “Local Stability of Laser-Welded Stainless-Steel T-Section Stub Columns”. *Journal of Structural Engineering*, 150(7), 04024062.
SAC (2021). GB/T 228-1:2021. Metallic materials – Tensile testing – Part 1: Method of test at room temperature, Standardization Administration of China (SAC).
Schafer, B. W. and S. Adany (2006). Buckling analysis of cold-formed steel members using CUFSM: Conventional and constrained finite strip methods. The 18th International Specialty Conference on Cold-Formed Steel Structures. Orlando**:** 39-54.
Shah, I. H., N. Hadjipantelis, L. Walter, R. J. Myers and L. Gardner (2023). “Environmental life cycle assessment of wire arc additively manufactured steel structural components.” *Journal of Cleaner Production*, 389.
Sun, Y. (2023). "The use of aluminum alloys in structures: Review and outlook." *Structures*, 57.
Sun, Y., Y. Liang and O. Zhao (2019). “Testing, numerical modelling and design of S690 high strength steel welded I-section stub columns.” *Journal of Constructional Steel Research*, 159 521-533.
Sun, Y. and O. Zhao (2019). “Material response and local stability of high-chromium stainless steel welded I-sections.” *Engineering Structures*, 178 212-226.
Sun, Y., W. Cheng and K. Chen (2024). “Experimental study of in-fire and post-fire material response of high-strength aluminium alloys.” *Journal of Building Engineering*, 91, 109581.
Sun, Y., M. Shao and K. Cashell (2025). “Postfire residual capacities of aluminum alloy unequal-leg angle sections.” *Journal of Structural Engineering*, 151(3), 04024224.
Wu, P., J. Wang and X. Wang (2016). “A critical review of the use of 3-D printing in the construction industry.” *Automation in Construction*, 68 21-31.
Zhang, R., L. Gardner, C. Buchanan, V.-P. Matilainen, H. Piili and A. Salminen (2021). “Testing and analysis of additively manufactured stainless steel CHS in compression.” *Thin-Walled Structures*, 159 107270.
Zhao, Y., Y. Chen, Z. Wang, J. Ye and W. Zhao (2023). “Mechanical properties, microstructural characteristics and heat treatment effects of WAAM stainless-steel plate material.” *Journal of Building Engineering*, 75.
Ziemian, R. D. (2010). “Guide to Stability Design Criteria for Metal Structures: Sixth Edition.” John Wiley & Sons.